Microscopic fields in liquid dielectrics

Daniel R. Martin and Dmitry V. Matyushov[a)]
Center for Biological Physics, Arizona State University, P.O. Box 871604, Tempe, Arizona 85287-1604, USA

(Received 27 August 2008; accepted 3 October 2008; published online 6 November 2008)

We present the results of an analytical theory and numerical simulations of microscopic fields in dipolar liquids. Fields within empty spherical cavities (cavity field) and within cavities with a probe dipole (directing field) and the field induced by a probe dipole in the surrounding liquid (reaction field) are considered. Instead of demanding the field produced by a liquid dielectric in a large-scale cavity to coincide with the field of Maxwell's dielectric, we continuously increase the cavity size to reach the limit of a mesoscopic dimension and establish the continuum limit from the bottom up. Both simulations and analytical theory suggest that the commonly applied Onsager formula for the reaction field is approached from below, with increasing cavity size, by the microscopic solution. On the contrary, the cavity and directing fields do not converge to the limit of Maxwell's dielectric. The origin of the disagreement between the standard electrostatics and the results obtained from microscopic models is traced back to the failure of the former to account properly for the transverse correlations between dipoles in molecular liquids. A new continuum equation is derived for the cavity field and supported by numerical simulations. Experimental tests of the theoretical results are suggested. © *2008 American Institute of Physics*. [DOI: 10.1063/1.3006313]

I. INTRODUCTION

Maxwell[1] used cavities carved in continuum to define the electric field **E** inside dielectrics. Lorentz instead used averages of microscopic fields over "physically infinitesimal" volumes to derive material Maxwell's equations.[2] Both approaches are different facets of the same question: How to relate microscopic fields within dielectrics to the macroscopic (Maxwell) field. This question, which has many ramifications in condensed-matter physics,[3] is certainly relevant to theories of dielectrics since any mean-field theory of dielectric response has to address the question of what is the local field acting on a liquid permanent or induced dipole. Debye's approach to this question[4] was to calculate the local field as a sum of the macroscopic field **E** and the field of liquid dipoles proportional, on average, to the dipolar polarization **P**:

$$\mathbf{E}_{\mathrm{loc}} = \mathbf{E} + \kappa \mathbf{P}, \tag{1}$$

where the coefficient κ, which we will call the "depolarization coefficient," needs to be determined from dielectric theories.

The polarization field **P** in Eq. (1) is related, on one hand, to the dielectric constant and, on the other hand, to the density of dipoles induced in the liquid,

$$\mathbf{P} = \frac{\epsilon - 1}{4\pi}\mathbf{E} = \rho\alpha\mathbf{E}_{\mathrm{loc}}. \tag{2}$$

Here, ρ is the number density and α is the molecular polarizability which is equal to the dipolar polarizability for induced dipoles and to $\beta m^2/3$ for permanent dipoles m; β is the inverse temperature. Only permanent dipole moments are considered in the rest of our discussion and so the dipolar polarizability is set equal to zero.

The equation for the local field follows from Eqs. (1) and (2),

$$\mathbf{E}_{\mathrm{loc}} = (1 - \kappa\rho\alpha)^{-1}\mathbf{E}. \tag{3}$$

Also, the dielectric constant derived from Eqs. (1) and (2),

$$\epsilon = 1 + \frac{4\pi\rho\alpha}{1 - \kappa\rho\alpha}, \tag{4}$$

anticipates the possibility of a polarization catastrophe at $\kappa\rho\alpha = 1$. When $\kappa\rho\alpha > 1$, the system becomes globally unstable, $\epsilon < 0$, and transition to the ferroelectric phase is expected, i.e., a spontaneous creation of a net dipolar polarization without an external electric field. A relation similar to Eq. (4) can be written for the k-dependent response. If $\epsilon(k)$ becomes negative at some values of k,[5] the system is globally stable but becomes unstable to some excitations; polarization waves[6] and Cooper pairs[3] are the examples.

The choice $\kappa = 4\pi/3$ corresponds to the Lorentz local field[4]

$$\mathbf{E}_{\mathrm{loc}} = \mathbf{E}_L = \frac{\epsilon + 2}{3}\mathbf{E}. \tag{5}$$

While this choice of κ is generally accepted in the theory of ferromagnetism (Weis theory), its counterpart for electric dipoles leads to the Debye equation[4] predicting ferroelectric order at the dipolar density $y = 1$,

[a)]Electronic mail: dmitrym@asu.edu.

$$y = \frac{\epsilon - 1}{\epsilon + 2}, \tag{6}$$

where $y=(4\pi/9)\beta\rho m^2$. Since many polar liquids are paraelectric at $y>1$, alternative definition of the depolarization coefficient in Eq. (1) is required.

Onsager[7] suggested that the depolarization coefficient should decrease with increasing dielectric constant as follows:

$$\kappa(\epsilon) = 4\pi(2\epsilon + 1)^{-1}, \tag{7}$$

which results in the Onsager relation when substituted into Eq. (4):

$$y = \frac{(\epsilon - 1)(2\epsilon + 1)}{9\epsilon}. \tag{8}$$

Even though local correlations, incorporated into the Kirkwood factor g_K,[8] were missing from Onsager's formulation, the theory has enjoyed success because of the destructive effect of molecular quadrupoles on the local dipolar order, making the Kirkwood factor close to 1 for many molecular liquids.[4,8]

The Onsager depolarization function $\kappa(\epsilon)$, which coincides with the Lorentz approach only at $\epsilon=1$, leads to the local field equal to the field inside a physical spherical cavity carved from the dielectric[4] (cavity field $\mathbf{E}_c^{\text{cont}}$),

$$\mathbf{E}_{\text{loc}} = \mathbf{E}_c^{\text{cont}} = \frac{3\epsilon}{2\epsilon + 1}\mathbf{E}. \tag{9}$$

We will dub E_c^{cont} as the Maxwell cavity field throughout below since it follows from the solution of the Maxwell material equations for a spherical cavity in a uniformly polarized dielectric.[9,10]

The Onsager formulation has eliminated the ferroelectric transition from the theory. This result has been recently challenged by computer simulations which had produced ferroelectric phase in model dipolar fluids.[11–13] It was also found that the result is sensitive to the boundary conditions employed in the simulation protocol,[14] i.e., to the magnitude of the depolarization field, a result known since the calculations by Luttinger and Tisza[15] of dipolar crystals. It is still not entirely clear if these model results are transferable to molecular polar liquids.[16–18]

On the theoretical side, Ramshaw[19] and Høye and Stell[20] extended Debye's equation to

$$\frac{\epsilon - 1}{\epsilon + 2} = y[1 - (\rho/3)\tilde{c}^{110}(0)]^{-1}, \tag{10}$$

where $\tilde{c}^{110}(k)$ is the projection of the inverted-space direct correlation function on the scalar product rotational invariant.[8] The existence of the ferroelectric transition, $\rho\tilde{c}^{110}(0)=3$, is then fully determined by the short-range dipolar correlations[21] which are still hard to determine accurately by analytical techniques.[22]

An important question lingering behind many of these developments, which has remained mostly unanswered, is to what extent continuum electrostatics can be applied to the calculation of the microscopic fields within dielectrics: $\mathbf{E}_{\text{loc}}$, $\mathbf{E}_c$, and, in addition, the reaction field $\mathbf{R}$ central to the Onsager theory and its applications to spectroscopy and solvation.[23] The local field $\mathbf{E}_{\text{loc}}$ is by definition a mean-field construct and can in fact be different from the Onsager directing field[4,7] $\mathbf{E}_d$. The latter is the difference of the total microscopic field $\mathbf{E}_{\text{mic}}$ acting on a dipole inside a dipolar liquid and the reaction field $\mathbf{R}$ which does not contribute to the torque rotating the dipole in the external field of the dielectric experiment.

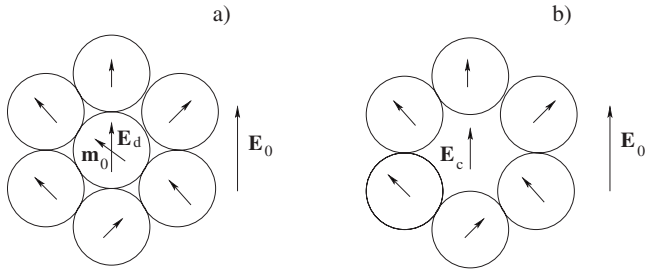

FIG. 1. (a) Onsager's directing field $\mathbf{E}_d$ inside a dipolar liquid and the (b) cavity field $\mathbf{E}_c$ inside a physical cavity carved in the liquid placed in the uniform external field $\mathbf{E}_0$. The local field $\mathbf{E}_{\text{loc}}$ [Eq. (3)] is a mean-field approximation for $\mathbf{E}_d$. $\mathbf{m}_0$ is the dipole moment of a target molecule.

Both the local and directing fields might, in turn, differ from the field inside a physical cavity. In the latter case, the existence of a physical interface might modify the local density profile and/or dipolar correlations compared to the situation when a molecule within a homogeneous liquid is considered (Fig. 1). The cavity field can in fact be defined as the directing field in the limit of zero target dipole ($\mathbf{m}_0$ in Fig. 1) inside the excluded volume, which is usually the repulsive core of a target molecule.

This paper analyzes the distinctions between these different dielectric fields from the perspective of both the microscopic liquid-state theories and numerical simulations. Apart from examining the microscopic fields in fluid dielectrics, our study allows us to gain insights into a more general question of the convergence of the dielectric properties of molecular liquids to those anticipated by the standard continuum electrostatics. The study thus asks the following question: how far is the physical system of a fluid dielectric from the mathematical construct of Maxwell's dielectric?

II. CALCULATION OF FIELDS IN DIELECTRICS

A. Formalism

In order to set up the calculation of the dielectric response in terms of microscopic properties of dielectrics, we will consider the Gaussian generating functional for the dipolar polarization field $\mathbf{P}$:[24,25]

$$G(\mathbf{A}) = \int e^{\mathbf{A}*\mathbf{P} - \beta H_{\text{B}}[\delta\mathbf{P}]} \prod_{\Omega_0} \delta[\mathbf{P}(\mathbf{r})] \mathcal{D}\mathbf{P}. \tag{11}$$

Asterisk between two vector fields refers to both the space integration and tensor contraction. When asterisk connects fields with tildes, as in $\tilde{\mathbf{E}}*\tilde{\mathbf{P}}$, this stands for the integration in inverted space of the scalar product of two Fourier transforms $\tilde{\mathbf{E}}$ and $\tilde{\mathbf{P}}$ of the fields $\mathbf{E}$ and $\mathbf{P}$, respectively. Further, in Eq. (11), $H_{\text{B}}[\delta\mathbf{P}]$ is the Hamiltonian of the polarization fluc-

tuations $\delta\mathbf{P}$ characterized by the response function of the pure isotropic solvent $\boldsymbol{\chi}_s(\mathbf{k})$,

$$H_B[\delta\mathbf{P}] = \tfrac{1}{2}|\delta\tilde{\mathbf{P}}|^2 * \boldsymbol{\chi}_s^{-1}. \tag{12}$$

The product of δ functions in Eq. (11) excludes the polarization field, over which the functional integral is taken, from some volume Ω_0 within the liquid.[24] This volume can specify the cavity in the dielectric for the cavity field calculations or the volume of a given target molecule for the calculation of directing/microscopic fields in the bulk dielectric. To combine these two possibilities, we will call the volume Ω_0 the "solute volume."

The constraint imposed on the polarization field to vanish from the solute space modifies the response function from that of the pure solvent $\boldsymbol{\chi}_s(\mathbf{k}_1)$ to a nonlocal response function $\boldsymbol{\chi}(\mathbf{k}_1,\mathbf{k}_2)$ depending on two wave vectors.[26] This function is obtained by taking the second derivative of $\ln[G(\mathbf{A})]$ in the auxiliary field $\mathbf{A}$ and setting $\mathbf{A}=0$. The result is

$$\boldsymbol{\chi}(\mathbf{k}_1,\mathbf{k}_2) = \boldsymbol{\chi}_s(\mathbf{k}_1)\delta_{\mathbf{k}_1,\mathbf{k}_2} - \boldsymbol{\chi}^{\mathrm{corr}}(\mathbf{k}_1,\mathbf{k}_2), \tag{13}$$

where the correction response function $\boldsymbol{\chi}^{\mathrm{corr}}(\mathbf{k}_1,\mathbf{k}_2)$ accounts for the effect of the solute excluding the polarization field from its volume. This second component is given by the following equation:

$$\boldsymbol{\chi}^{\mathrm{corr}}(\mathbf{k}_1,\mathbf{k}_2) = \boldsymbol{\chi}''(\mathbf{k}_1)\theta_0(\mathbf{k}_1-\mathbf{k}_2)\cdot\boldsymbol{\chi}_s(\mathbf{k}_2). \tag{14}$$

Here, θ_0 is the Fourier transform of the step function limiting the solute volume

$$\theta_0(\mathbf{k}) = \int_{\Omega_0} e^{i\mathbf{k}\cdot\mathbf{r}}d\mathbf{r} \tag{15}$$

and the response function $\boldsymbol{\chi}''(\mathbf{k})$ is given as a sum of projections on longitudinal, $\mathbf{J}^L=\hat{\mathbf{k}}\hat{\mathbf{k}}$, and transverse, $\mathbf{J}^T=\mathbf{1}-\hat{\mathbf{k}}\hat{\mathbf{k}}$, dyads,

$$\boldsymbol{\chi}'' = \mathbf{J}^L\chi''^L + \mathbf{J}^T\chi''^T. \tag{16}$$

Here and below, hats over bold characters denote unit vectors. Further, in Eq. (16), the scalar response functions $\chi''^{L,T}$,

$$\chi''^{L,T} = \frac{S^{L,T}}{S^{L,T}-\chi'^{L,T}}, \tag{17}$$

are given in terms of the structure factors of the longitudinal and transverse polarization fluctuations, $S^L(k)$ and $S^T(k)$, and the response functions $\chi'^{L,T}$ are specified below.

The polarization structure factors (Fig. 2) enter the response function of the homogeneous dipolar liquid in Eq. (12) in the form of two orthogonal, longitudinal, and transverse, projections,[27]

$$\boldsymbol{\chi}_s(\mathbf{k}) = \frac{3y}{4\pi}[S^L(k)\mathbf{J}^L + S^T(k)\mathbf{J}^T]. \tag{18}$$

The structure factor functions are obtained by averaging the projections of unit dipole vectors $\hat{\mathbf{e}}_j$ on an arbitrary chosen wave vector $\hat{\mathbf{k}}$ according to the equations

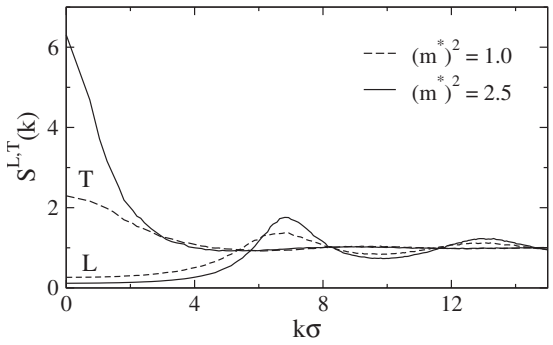

FIG. 2. Longitudinal (L) and transverse (T) structure factors of the dipolar hard-sphere liquid from numerical simulations at $\rho^*=0.8$ and $(m^*)^2=2.5$ (solid lines, $\epsilon=53.7$) and 1.0 (dashed lines, $\epsilon=8.52$).

$$S^L(k) = \frac{3}{N}\langle\sum_{i,j}(\hat{\mathbf{e}}_i\cdot\hat{\mathbf{k}})(\hat{\mathbf{k}}\cdot\hat{\mathbf{e}}_j)e^{i\mathbf{r}_{ij}\cdot\mathbf{k}}\rangle,$$
$$S^T(k) = \frac{3}{2N}\langle\sum_{i,j}[(\hat{\mathbf{e}}_i\cdot\hat{\mathbf{e}}_j)-(\hat{\mathbf{e}}\cdot\hat{\mathbf{k}})(\hat{\mathbf{k}}\cdot\hat{\mathbf{e}}_j)]e^{i\mathbf{r}_{ij}\cdot\mathbf{k}}\rangle, \tag{19}$$

where $\mathbf{r}_{ij}=\mathbf{r}_i-\mathbf{r}_j$ and N is the number of particles in a polar liquid. Their $k=0$ values are related to the dielectric constant as follows:[8]

$$S^L(0) = \frac{\epsilon-1}{3y\epsilon},$$
$$S^T(0) = \frac{\epsilon-1}{3y}. \tag{20}$$

Equation (20) can be viewed as a microscopic definition of the dielectric constant. This definition thus does not require assuming the locality of the response entering the electrostatic constitutive relation [left-hand side of Eq. (2)] and does not involve problems related to the dependence of the result on the sample shape.[28] In addition, the trace $g_K=(1/3)[S^L(0)+2S^T(0)]$ is the Kirkwood g factor, and Eq. (20) leads to the Kirkwood–Onsager equation

$$yg_K = \frac{(\epsilon-1)(2\epsilon+1)}{9\epsilon}. \tag{21}$$

The projections $\chi'^{L,T}$ in the denominator in Eq. (17) renormalize the dielectric response by excluding the dipolar polarization field from the volume of the solvent. They can be expressed through projections of the pair distribution function of the homogeneous dipolar liquid on rotational invariants,[26]

$$\chi'^L(k) = (\rho/3)\int_{\Omega'} d\mathbf{r}[h^{110}(r)j_0(kr) - 2h^{112}(r)j_2(kr)],$$
$$\chi'^T(k) = (\rho/3)\int_{\Omega'} d\mathbf{r}[h^{110}(r)j_0(kr) + h^{112}(r)j_2(kr)]. \tag{22}$$

Here, for a spherical solute of radius R_0, Ω' is the volume outside of a sphere of the radius $2R_1$, where

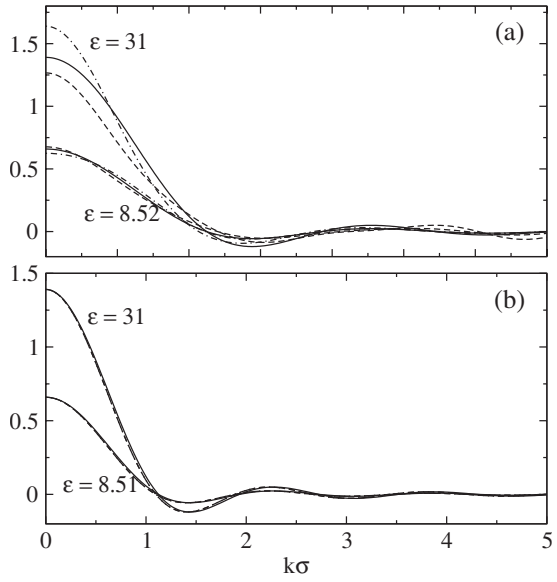

FIG. 3. Response functions $-\chi'^{L}(k)/2$ (dashed lines) and $\chi'^{T}(k)$ (dashed-dotted line) calculated from Eq. (22) and compared to $A(k)$ [solid line, see Eqs. (25) and (26)]. The upper curves are obtained at $\epsilon=31$, $(m^*)^2=2.0$, while the lower curves refer to $\epsilon=8.52$, $(m^*)^2=1.0$; $\rho^*=0.8$. The $h^{110}(k)$ and $h^{112}(k)$ projections required for the integration in Eq. (22) have been obtained from MC simulations. Panels (a) and (b) correspond to $R_0/\sigma=0.5$ and 1.5, respectively.

$$R_1 = R_0 + \sigma/2 \tag{23}$$

is the distance of the closest approach of the liquid molecule of diameter σ to the solute repulsive core. The functions $h^{110}(r)$ and $h^{112}(r)$ in Eq. (22) are the projections of the orientation-dependent pair distribution function of the homogeneous dipolar liquid on rotational invariants.[8,29]

The functions $\chi'^{L,T}$, defined by Eq. (22), are affected by two types of correlations in the liquid, the short-range correlations expressed by the projection $h^{110}(r)$ and, partially, by $h^{112}(r)$ and long-range dipolar correlations represented by the long-distance asymptote of $h^{112}(r)$:[8]

$$\rho h^{112}(r) \simeq \frac{(\epsilon-1)^2}{4\pi y\epsilon}\frac{1}{r^3}. \tag{24}$$

If the short-range correlations are neglected and only the long-range asymptote of $h^{112}(r)$ is left in Eq. (22), one easily gets

$$\chi'^{L}(k) = -2A(k), \quad \chi'^{T} = A(k), \tag{25}$$

where

$$A(k) = \frac{(\epsilon-1)^2}{3\epsilon y}\frac{j_1(2kR_1)}{2kR_1}. \tag{26}$$

Since integration in Eq. (22) extends beyond the distance $r>2R_1$, the short-range correlations do not contribute much to the integral in Eq. (22) and approximation (25) is fulfilled quite well even for the cavity size equal to that of the liquid molecule [Fig. 3(a)]. This approximation becomes increasingly accurate with growing cavity [see Figs. 3(a) and 3(b)] making the replacement in Eq. (25) very accurate for most practical calculations.

B. Cavity field

We now consider a spherical cavity inside a dielectric liquid and use the response function from Eqs. (13) and (14) to determine the cavity field. Considering dielectric placed in a uniform external field $\mathbf{E}_0$, we can obtain the projection of the field inside the cavity on the direction of that external field, $\hat{\mathbf{e}}_0=\mathbf{E}_0/E_0$:

$$E_c = E_0 + \hat{\mathbf{e}}_0 \cdot \tilde{\mathbf{T}} * \boldsymbol{\chi} * \tilde{\mathbf{E}}_0 \cdot \hat{\mathbf{e}}_0. \tag{27}$$

Here, $\tilde{\mathbf{E}}_0=\mathbf{E}_0\delta_{\mathbf{k},\mathbf{0}}$ is the Fourier transform of the external field and $\tilde{\mathbf{T}}$ is the Fourier transform of the dipole-dipole interaction tensor excluding the hard core of the solute with the radius of closest approach R_1 [Eq. (23)]:

$$\tilde{\mathbf{T}} = -4\pi\mathbf{D}_{\mathbf{k}}\frac{j_1(kR_1)}{kR_1}, \tag{28}$$

where $\mathbf{D}_{\mathbf{k}}=3\hat{\mathbf{k}}\hat{\mathbf{k}}-\mathbf{1}$ and $j_n(x)$ is the spherical Bessel function of order n.

Substituting $\boldsymbol{\chi}$ from Eq. (13) to Eq. (27) one gets

$$\frac{E_c}{E_0} = \frac{\epsilon+2}{3\epsilon} - \hat{\mathbf{e}}_0 \cdot \tilde{\mathbf{T}} * \boldsymbol{\chi}^{\mathrm{corr}}(\mathbf{k},0) \cdot \hat{\mathbf{e}}_0. \tag{29}$$

The first term in this equation is the Lorentz field[4] [Eq. (5)] which appears in our formalism as the field inside small cavities[30] of size much smaller than the length of dipolar correlations in the liquid. This result is in line with the definition of the Lorentz field used by Ramshaw.[19] The opposite limit of macroscopically large cavities turns out to be trickier to derive.

For a spherical cavity, the Fourier transform of the cavity step function $\theta_0(k)$ in Eq. (15) becomes

$$\theta_0(k) = 4\pi R_1^3\frac{j_1(kR_1)}{kR_1}. \tag{30}$$

Therefore, combining Eqs. (14), (28), and (30) and using Eq. (20) in Eq. (18) to obtain $\boldsymbol{\chi}_s(0)$, one gets

$$\frac{E_c}{E_0} = \frac{\epsilon+2}{3\epsilon} - \frac{4R_1}{3\pi}\frac{\epsilon-1}{\epsilon}\int_0^\infty j_1^2(kR_1)(\chi''^{T}(k)-\chi''^{L}(k))dk. \tag{31}$$

The presence of a cavity alters the response functions $\chi''^{L,T}$ through $\chi'^{L,T}$ in the denominator of Eq. (17); if this component is neglected, the second integral in Eq. (31) vanishes, resulting in the Lorentz field.

The continuum limit of a macroscopically large cavity is now obtained by assuming that the functions $\chi''^{L,T}(k)$ do not change in the range of k values, $k\simeq 2\pi/R_1$, in which $j_1^2(kR_1)$ decays and, therefore, by replacing $\chi''^{L,T}(k)$ with their $k=0$ values, $\chi''^{L,T}(0)$. This immediately leads to the result of continuum electrostatics:[4]

$$\frac{E_c^{\mathrm{cont}}}{E_0} = \frac{3}{2\epsilon+1}. \tag{32}$$

Our formulation therefore contains two well-established limits: the field inside small cavities, much smaller that the length scale of dipolar correlations (Lorentz field), and the

field inside macroscopic cavities for which macroscopic electrostatics apply [Eq. (32)]. However, it is easy to realize that there are problems with the derivation of Eq. (32) for cavities of finite size. First, it is not clear if the $k=0$ limit can be applied to both $S^{L,T}(k)$ and $\chi'^{L,T}(k)$ in Eq. (17) since $\chi'^{L,T}(k)$ decay on about the same scale of k as does $j_1^2(kR_1)$ in Eq. (31). Second, whereas the longitudinal structure factor is reasonably flat at small k values, the transverse structure factor decays very sharply from its $k=0$ value, approaching delta function at the ferroelectric transition (Fig. 2). The application of the continuum limit to the transverse part of the response is therefore not well justified. This problem is clearly seen in the fact that $\chi''^{T}(k)-\chi''^{L}(k)$ can be rewritten as

$$\chi''^{T}(k)-\chi''^{L}(k)=\frac{\chi'^{T}}{S^{T}-\chi'^{T}}-\frac{\chi'^{L}}{S^{L}-\chi'^{L}}. \tag{33}$$

When Eq. (25) [$\chi'^{L}(k)=-2A(k)$ and $\chi'^{T}=A(k)$] is used in Eq. (33), the oscillatory function $A(k)$ [Eq. (26)] becomes a part of the integral. If now the continuum $k=0$ substitute is used only for the denominators in Eq. (33), one gets an alternative "continuum limit" for the cavity field:

$$\frac{E_c^{\mathrm{cont}}}{E_0}=\frac{7(\epsilon+1)^2+8\epsilon}{12\epsilon(2\epsilon+1)}. \tag{34}$$

This cavity field does not decay to zero with increasing ϵ but instead saturates at 7/24, implying that the ability of a polar liquid to screen the external field is not unlimited as Eq. (32) would suggest.

The main result of this calculation is the realization that the definition of the dielectric continuum is based on the smallness of the ratio of the correlation length of dipolar interactions in the liquid to the physical size of the cavity. Since the dipolar correlation length depends on solvent polarity, in particular, for transverse response, the definition of continuum for a given cavity size may vary depending on the polarity range considered. In fact, the full calculation according to Eq. (31) predicts branching between two continuum solutions through a point of singularity.

Figure 4 shows the results of calculating the cavity field from Eq. (31) using the response functions $\chi''^{L,T}$ from our Monte Carlo (MC) simulations (points). The range of numerical calculations is limited since, with growing ϵ, the response function $\chi''^{L}(k)$ gains a real-axis singularity corresponding to a real solution k^* of the equation

$$S^{L}(k^*)-\chi'^{L}(k^*)=0. \tag{35}$$

The real-axis singularity signals the appearance of a nondecaying polarization wave induced by the cavity and radially propagating from it through the entire liquid. This longitudinal polarization wave is terminated at the boundary of a dielectric sample where it creates surface charges. In reality, it may terminate at the surface of a polar domain of a nanoscale dimension as suggested by Shelton's hyper-Rayleigh scattering experiments.[16,17]

Because of the real-axis singularity, numerical integration cannot be done in the range of parameters where a solution k^* in Eq. (35) exists. The integral should be replaced with pole calculus, which requires an analytical solution for

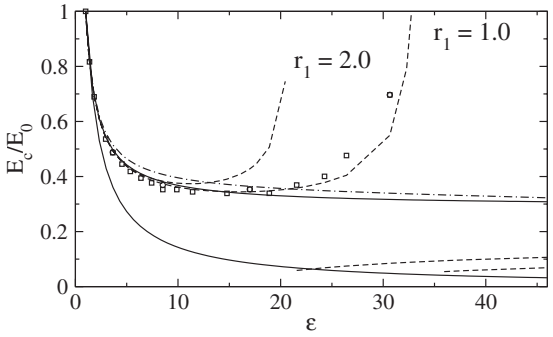

FIG. 4. Cavity field calculated from Eq. (31) with two cavity sizes indicated by the distance of the closest approach, $r_1=R_0/\sigma+0.5$, in the plot. The points were obtained by numerical integration in Eq. (31) with $S^{L,T}(k)$ from MC simulations ($r_1=1.0$), while the dashed lines refer to the calculations using the parametrized MSA (Ref. 31). The integral is calculated numerically before the appearance of the singularity on the real axis [Eq. (35)] and by summation over the poles when the singularity falls on the axis. The two methods give identical results when numerical integration is justified. The upper and lower solid lines refer to two continuum limits, Eqs. (34) and (32), respectively. The dashed-dotted line refers to the lattice summation [Eq. (36)] instead of continuous integration in Eq. (31) taken for a cubic cell of $N=108$, $r_1=2.0$.

$\chi''^{L}(k)$. This calculation, shown by the dashed lines in Fig. 4, was done by using expressions (25) and (26) for $\chi'^{L,T}$ and parametrized mean-spherical approximation (MSA) (Ref. 29) solution for $S^{L,T}(k)$.[31] This approximation corrects the MSA polarization structure factors by requiring them to satisfy the $k=0$ results given by Eq. (20). The dielectric constant at each dipole moment is taken from our MC simulations.

The calculations done by both pole summation and by numerical integration in the range of polarities before the appearance of the singularity are in good agreement with each other and with the numerical calculations using the response functions from simulations (points in Fig. 4). Only pole summation applies after the singularity falls on the real axis, and it shows a discontinuous drop of the cavity field to the level close to the macroscopic solution given by Eq. (32).

In order for the solution to switch to the ordinary macroscopic limit, the singularity k^* should be a part of the sample's spectrum of wavenumbers. The spectrum of $\mathbf{k}$ is limited to a discrete set of lattice values for a finite-size sample, and it is hardly possible for k^* to coincide with one of the lattice vectors. Indeed, when continuous k integration in Eq. (12) is replaced with the lattice sum according to the rule

$$\int d\mathbf{k}/(2\pi)^3 \rightarrow L^{-3}\sum_{n,l,m}, \tag{36}$$

we do not observe a rising part of the cavity field (dashed-dotted line in Fig. 4). In Eq. (36), L is the size of the cubic lattice and the lattice wave vectors are $(2\pi/L)\{n,l,m\}$. As expected from this calculation, we in fact have not observed switching to the ordinary continuum in our finite-size numerical simulations (see below).

C. Reaction field

The reaction field $\mathbf{R}$ is produced by the liquid polarization induced by the dipole moment $\mathbf{m}_0$ of a target molecule

(solute, Fig. 1). It is parallel to the dipole moment $\mathbf{m}_0$, resulting in the free energy of dipole stabilization (solvation chemical potential) $\mu_{0s}=-m_0R/2$. Since the response function of a polar liquid follows from the generating functional in Eq. (11), the reaction field can also be obtained from the formalism outlined above after replacing the uniform external field with the field of a point dipole $\tilde{\mathbf{E}}_0$. The chemical potential of solvation μ_{0s} is then given by a simple relation,[26]

$$\mu_{0s}=\frac{3}{2\epsilon+1}[\epsilon\mu_{0s}^{L}+\mu_{0s}^{T}], \tag{37}$$

where the longitudinal and transverse components of the solvation free energy are

$$-\mu_{0s}^{L,T}=(3y/8\pi)|\tilde{\mathbf{E}}_0^{L,T}|^2 * S^{L,T}(k). \tag{38}$$

Here, as above, the asterisk implies the inverted-space integration.

When the dipolar field is substituted into Eqs. (37) and (38), one gets for the reaction field R

$$R=\frac{12ym_0}{\pi R_1^2(2\epsilon+1)}\int_0^\infty j_1^2(kR_1)[2\epsilon S^L(k)+S^T(k)]dk. \tag{39}$$

If the k dependence of the structure factors in Eq. (39) is neglected, one arrives at the standard Onsager solution for the reaction field,[7]

$$R^{\mathrm{cont}}=\frac{2m_0}{R_1^3}\frac{\epsilon-1}{2\epsilon+1}. \tag{40}$$

Therefore, the continuum Onsager result is the $k=0$ limit of the microscopic equations and no new solution occurs, in contrast to the case with the cavity field.

The cavity radius is not specified in continuum models, but the common practice suggests to use the hard-sphere radius R_0 instead of the radius of the solvent-accessible sphere R_1 in Eq. (40). Other parametrizations, commonly resulting in effective radii between R_0 and R_1, are of course also possible. In particular, perturbation models of dipole solvation[32,33] suggest the following expression for the effective cavity radius:

$$R_{\mathrm{eff}}^{-3}=3\int_0^\infty g_{0s}(r)(dr/r^4), \tag{41}$$

where $g_{0s}(r)$ is the solute-solvent radial pair distribution function. The effective radius $R_{\mathrm{eff}}(r_1,\rho^*)$ as a function of $r_1=R_0/\sigma+0.5$ and the solvent reduced density ρ^* were tabulated in terms of simple polynomial functions in Refs. 33 and 34 by using the hard-sphere approximation for $g_{0s}(r)$ in Eq. (41).

D. Microscopic field

The local field E_{loc} defined in Eqs. (1)–(3) above represents the mean-field approximation for the directing field, i.e., the field acting on a given dipole from a dielectric uniformly polarized by an external electric field. Following Onsager,[7] we will distinguish the directing field from the actual microscopic electric field created by both the polarized dielectric and the polarization induced in the surroundings by the target dipole itself, the Onsager reaction field.[7] All these considerations are commonly applied to homogeneous polar liquids. We instead approach the problem here from a somewhat more general perspective considering a probe dipole $\mathbf{m}_0$ at the center of a spherical cavity with the radius R_0 immersed in a uniformly polarized dipolar liquid (Fig. 1).

Assuming that a weak external field produces a linear perturbation of the system, it is straightforward to show that the microscopic field E_{mic} in the direction of the uniform external field is a sum of the field created by the polarized dielectric at the position of the molecule, E_d, and the average projection of the reaction field $\mathbf{R}$ on the direction of the external field $\hat{\mathbf{e}}_0$:

$$E_{\mathrm{mic}}=E_d+\langle\hat{\mathbf{e}}_0\cdot\mathbf{R}\rangle. \tag{42}$$

Here, the angular brackets denote a statistical average over the perturbed Hamiltonian $H=H_0-\mathbf{M}\cdot\mathbf{E}_0$, where H_0 is the Hamiltonian of the system without the uniform external field $\mathbf{E}_0$ and $\mathbf{M}$ is the total dipole moment of the system.

Since the reaction field is always parallel to the target's dipole, Onsager's directing field E_d in Eq. (42) is responsible for the torque rotating the dipole in an external electrical field and is ultimately connected to the dielectric response. Field E_d has the physical meaning of a "virtual" cavity field when no real interface exists in the liquid. It should in principle be distinguished from the actual cavity field E_c when such an interface exists, even though these two fields are often considered equal, as in the Onsager formulation [Eq. (9)].

Since the reaction field is directed along $\mathbf{m}_0$ such that $\mathbf{R}=f\mathbf{m}_0$, one gets

$$E_{\mathrm{mic}}=E_d+f(\beta m_0^2/3)g_K^{(0)}E_0, \tag{43}$$

where

$$g_K^{(0)}=1+\frac{m}{m_0}\sum_{j\neq 0}\langle\hat{\mathbf{m}}_0\cdot\hat{\mathbf{m}}_j\rangle_0 \tag{44}$$

and $\langle\cdots\rangle_0$ denotes an ensemble average in the absence of the external field.

The term $g_K^{(0)}$ [Eq. (44)] determines the angular correlation of the probe dipole with the dipoles in the dipolar solvent. It becomes the Kirkwood g factor in the case of a homogeneous liquid ($m_0=m$). By using the Maxwell cavity field from Eq. (9) and the Onsager reaction field from Eq. (40), one can obtain the continuum prediction for the microscopic field:

$$\frac{E_{\mathrm{mic}}}{E_0}=\frac{3}{2\epsilon+1}+\frac{2(\epsilon-1)}{2\epsilon+1}\left(\frac{m_0}{m}\right)^2\left(\frac{\sigma}{2R_0}\right)^3\frac{yg_K^{(0)}}{\eta}, \tag{45}$$

where $\eta=(\pi/6)\rho\sigma^3$ is the liquid packing fraction. In the case of a homogeneous liquid with $m_0=m$ and $2R_0=\sigma$ one can use the Kirkwood–Onsager equation [Eq. (21)] with the result

$$\frac{E_{\mathrm{mic}}}{E_0}=\frac{3}{2\epsilon+1}+\frac{2(\epsilon-1)^2}{9\eta\epsilon}. \tag{46}$$

This equation predicts that at large polarities the microscopic field scales linearly with the dielectric constant with the

slope $2/9\eta$. In the opposite limit of large cavities, the correlation term $g_K^{(0)}$ is expected to tend to unity and the corresponding continuum solution becomes

$$\frac{E_{\mathrm{mic}}}{E_0} = \frac{3}{2\epsilon+1} + \frac{2(\epsilon-1)^2}{9\eta\epsilon g_K}\left(\frac{m_0}{m}\right)^2\left(\frac{\sigma}{2R_0}\right)^3. \quad (47)$$

III. MONTE CARLO SIMULATIONS

The discussion above has focused on macroscopic systems in the thermodynamic limit $N\to\infty$. Given different continuum limits achievable for the cavity field, it is not entirely clear if periodic systems commonly employed in numerical simulations[35] can adequately describe the macroscopic limit for dielectric fields in a system with long-range dipolar interactions. The fact that simulations converge to a certain limit at $N\to\infty$ does not necessarily guarantee that this is the same limit as seen in the laboratory dielectric experiment. Here, we present the results of MC simulations within the standard protocol of periodically replicated simulation cell.

MC simulations have been carried out in the standard *NVT* Metropolis algorithm, periodic boundary conditions, and cutoff of the dipolar forces at the half of the cubic box length. The dielectric constants of the homogeneous fluids were calculated using Neumann's formalism[36] as implemented in our previous studies.[33] The initial configuration was set up as a face-centered cubic lattice with random dipolar orientations and varied number of particles, N. While this configuration was directly used for the homogeneous liquid simulations, the hard-sphere solute/cavity was "grown" in the cell center for the cavity field simulations. This was done starting from an initial diameter of 0.5σ and increasing the diameter at each step by 0.002σ, adjusting σ so as to ensure constant density $\rho^*=\rho\sigma^3=0.8$, and moving and rotating the solvent particles according to the Metropolis algorithm. After the solute/cavity was constructed, the initial configuration was equilibrated for approximately 10^5-10^6 steps in parallel (using OPENMPI) assuring that each processor started from a different point along the Markov chain. The parallel part of the program was implemented by running the same MC program on different processors separately. A linear scaling with the number of processors was achieved. The production runs of $(1-5)\times10^6$ steps were carried out for each $(m^*)^2$ and cavity size. Reaction field corrections were used for the dipolar interactions to speed up the simulations and were checked to give the results identical to applying Ewald sums.

The calculation of microscopic fields in dielectrics from numerical simulations requires caution in a proper treatment of the corrections for the cutoff of long-range dipolar interactions.[36] The cavity field was calculated from the linear response approximation:

$$E_c/E_0 = 1 + (\beta/3)\langle\delta\mathbf{E}_s\cdot\delta\mathbf{M}\rangle_0 - E_{\mathrm{corr}}. \quad (48)$$

Here, $\delta\mathbf{M}$ is the fluctuation of the total dipole moment of the simulation cell and $\delta\mathbf{E}_s$ is the fluctuation of the electric field produced by the liquid dipoles, $\mathbf{E}_s=\Sigma_j\mathbf{T}_j\cdot\mathbf{m}_j$, where $\mathbf{T}_j$ is the dipolar tensor responsible for the electric field of dipole j at the cavity center. The fact that a dipolar tensor with the reaction field cutoff appears in the simulation protocol requires the correction term E_{corr} in Eq. (48).

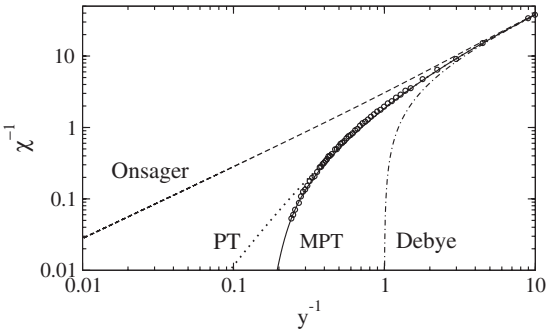

FIG. 5. The inverse dielectric susceptibility $\chi^{-1}=4\pi/(\epsilon-1)$ vs $1/y$. The points represent simulation data. The solid line refers to Eq. (51), and the dotted line refers to Eq. (50). The remaining two lines are the continuum results obtained from the Debye and Onsager equations, Eqs. (6) and (8), respectively. The solid line is obtained by fitting the parameter p in Eq. (51) to the simulation data with the best-fit value of $p=0.264$.

The microscopic field E_{mic} was obtained from simulations involving a probe dipole at the center of the cavity of radius R_0. The average projection of the liquid field at the cavity center on the direction of the probe dipole results in the reaction field response coefficient, $f=\langle\mathbf{E}_s\cdot\hat{\mathbf{m}}_0\rangle_0/m_0$, where $\langle\cdots\rangle_0$ implies an average over the configurations in equilibrium with a target dipole m_0 and in the absence of an external electric field. The microscopic field follows from the equation

$$\frac{E_{\mathrm{mic}}}{E_0} = \frac{E_d}{E_0} + (\beta m_0^2/3)g_K^{(0)}(f+f_{\mathrm{corr}}), \quad (49)$$

where the correction term f_{corr} accounts for the cutoff of the dipolar interactions. The explicit equations for the correction terms E_{corr} and f_{corr} in Eqs. (48) and (49) are given in the supplementary material.[37] Further, the directing field E_d in Eq. (49) is obtained from the simulated configurations with the target dipole m_0 by using Eq. (48). Since dipolar correlations around a target molecule are generally different from those around a physical cavity, the directing field turned out to deviate from the cavity field.

IV. RESULTS

A. Dielectric constant

The simulations performed here give access to the dielectric constant of the fluid of dipolar hard spheres. While they support the previously advocated idea of the existence of the ferroelectric transition in dipolar fluids,[11–13] our main focus here is on the local field defined through the dielectric constant by Eq. (3).

Figure 5 shows the inverse of the susceptibility $4\pi/(\epsilon-1)$ versus $1/y$. The Debye equation [Eq. (6)] is shown by the dashed-dotted line and the Onsager result [Eq. (8)] is given by the dashed line. As mentioned above, there is no ferroelectric transition in the Onsager equation. In addition, Fig. 5 shows the result of a perturbation expansion of the dielectric constant in terms of the dipolar density y as derived by Tani *et al.*,[38]

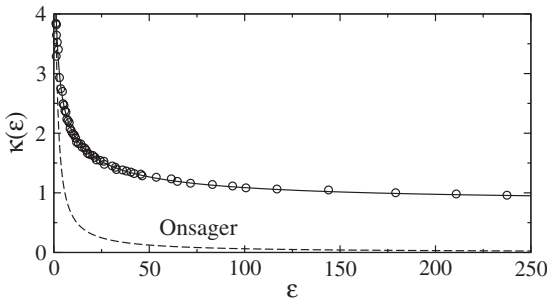

FIG. 6. The depolarization coefficient $\kappa(\epsilon)$ as a function of the dielectric constant ϵ for a dipolar fluid at $\rho^*=0.8$. The solid line is the fit to the simulation data (points) to Eq. (52). The dashed line is the Onsager result in Eq. (7).

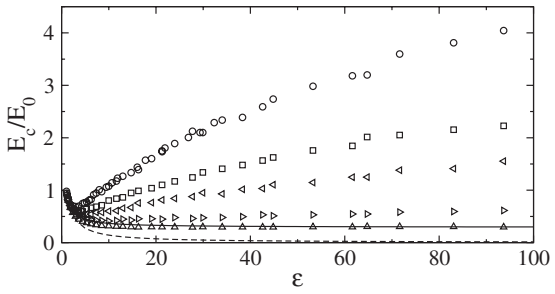

FIG. 7. The cavity field calculated from MC simulations with varying cavity size: $r_1=1.0$ ($N=108$, circles), 1.5 ($N=108$, squares), 2.0 ($N=256$, left triangles), 3.0 ($N=256$, right triangles), and 5.5 ($N=500$, up triangles). The solid line corresponds to the new continuum expression given in Eq. (34), while the dashed line refers to the standard Maxwell result [Eq. (32)].

$$\epsilon - 1 = 3y + 3y^2 + 3y^3 p. \tag{50}$$

We also show the result of the modified perturbation formula from Ref. 33,

$$\epsilon - 1 = 3y + 3y^2 + \frac{2}{p^2}(e^{3p^3y^3/2} - 1). \tag{51}$$

In Eqs. (50) and (51), p is related to the three-particle perturbation integral $I_{0s}^{(3)}$ tabulated in Ref. 38: $p=(9/16\pi^2)I_{0s}^{(3)}-1$.

The analytical equations are compared to the data taken from MC simulations (points in Fig. 5). It is obvious that both the Debye theory and the Onsager theory fail to predict the results of simulations. On the contrary both the perturbation theory [Eq. (50)] and modified perturbation theory (MPT) [Eq. (51)] do very well for smaller values of ϵ, while the MPT covers all the simulation data in the range $\epsilon \leq 300$. The perturbation expansion from Ref. 38 results in $p=0.252$ while the solid line in Fig. 5 is obtained using p as a fitting parameter with a close best-fit value of $p=0.264$.

Using the data from simulations one can fit the depolarization coefficient $\kappa(\epsilon)$ in Eq. (4) as a function of the dielectric constant. This representation of the data is more convenient than using the dielectric constant itself since $\kappa(\epsilon)$ tends to a constant limit with increasing polarity instead of diverging, as is the case with ϵ. A cubic Padé form was found to give a reasonable fit of the simulation data as shown in Fig. 6,

$$\kappa(\epsilon) = A\frac{1 + a_1\epsilon + b_1\epsilon^3}{1 + a_2\epsilon + b_2\epsilon^3}, \tag{52}$$

where the fitting parameters are $A=6.106$, $a_1=0.1701$, $b_1=0.000\,064\,2$, $a_2=0.7054$, and $b_2=0.000\,393$. The function $\kappa(\epsilon)$ from the Onsager model [Eq. (7), dashed line in Fig. 6] decays too fast compared to simulations, and the Debye theory would predict a constant value of $\kappa(\epsilon)=4\pi/3$. Taken together, Eqs. (4) and (52) give $\epsilon(y)$ in the entire paraelectric phase of the dipolar fluid by solving the equation

$$\epsilon = 1 + \frac{3y}{1 - (3y/4\pi)\kappa(\epsilon)}, \tag{53}$$

which is, however, less convenient than the direct application of Eq. (51).

The function $\kappa(\epsilon)$ saturates to unity at $\epsilon \to \infty$, suggesting that the ferroelectric transition occurs at $y^*=(4\pi/3)p'$ with $p'=1.0$. This value for p' is somewhat lower in comparison to $p'=1.256$ reported by Weis[39] and might be a result of a particular mean-field form of ϵ in Eq. (53) used to represent the results. The representation in terms of $\kappa(y)$ is not very convenient since it does not saturate to a clear limit. This function can, however, be useful for attempts to build mean-field theories of dipolar, also magnetic, systems and we provide here a fit of the simulation results to a Padé form:

$$\kappa(y) = \frac{4\pi}{3}\frac{1 + 0.008\,967\,9y}{1 + 0.923\,704y - 0.019\,673\,5y^2}, \tag{54}$$

which applies to the range $0 \leq y \leq 4$.

B. Cavity field

The simulation results for fields inside cavities of different sizes are shown in Fig. 7. All curves share the same basic dependence on polarity, showing a slow, almost linear increase with ϵ after an initial drop. This behavior is qualitatively similar to what has been obtained from the analytical theory in Fig. 4. However, the simulation results show no discontinuous drop at intermediate values of ϵ. Instead, the curves obtained by increasing the cavity size seem to level off and approach the continuum expression derived in Eq. (34) (solid line in Fig. 7).

There is, however, an indication that the cavity field might fall below the new continuum limit in Eq. (34) for specific values of $\{R_0, \epsilon\}$.[40] This observation can be seen in the inset in Fig. 8 which shows a slight decrease in the cavity field for $R_0/\sigma \geq 6$ and high values of ϵ. For smaller dielectric constants, this decrease in the cavity field is never observed.

There does appear some dependence on the number of particles used in the simulation when calculating the cavity field. Thus, separate simulations were used, increasing the number of particles each time and extrapolating to the $N \to \infty$ value. These extrapolated values for the cavity field are given in Table I in the supplementary material[37] with the corresponding number of particles used in each simulation given in the footnotes. Since extrapolation inevitably introduces errors, data at a given number N of particles in the simulation box were used in Figs. 7 and 8.

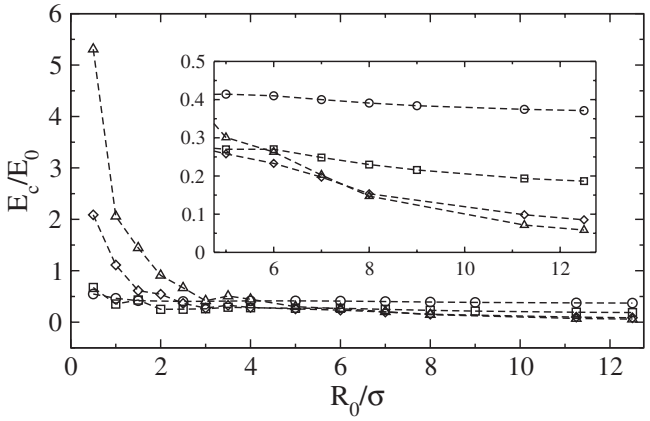

FIG. 8. The cavity field calculated directly from simulations [Eq. (48)] as a function of the cavity radius R_0/σ. The insrt is an expanded section at large R_0. The points represent $(m^*)^2=0.5$ (circles), 1.0 (squares), 2.0 (diamonds), and 3.0 (up triangles). The corresponding values of ϵ are 3.54, 8.52, 30.64, and 93.66.

Cavity fields obtained from the simulations clearly contradict the expectations from Maxwell's electrostatics. This contradiction might have two possible origins. First, it might be possible that the results obtained from simulations of periodic systems converge to some limit as the number of particles is increased, but this limit is different from that for a macroscopic system. We cannot investigate this possibility by current simulations. On the other hand, Maxwell's electrostatics is in fact a boundary condition problem. If the boundary conditions on the surface of dipolar liquids are different from those implicitly anticipated in deriving Maxwell's equations, one can get a different solution even in the limit of cavities much larger than the size of the liquid particles when conditions of macroscopic electrostatics are expected to apply. In order to investigate this second possibility, we have looked at the orientational structure of the liquid dipoles at the cavity/liquid interface.

We have studied the distance dependence of the second-rank orientational order parameter defined in terms of the projection of the unit dipole vector $\hat{\mathbf{e}}_j$ on the unit radius vector $\hat{\mathbf{r}}=\mathbf{r}/r$:

$$p_2(r)=\langle\sum_j P_2(\hat{\mathbf{r}}\cdot\hat{\mathbf{e}}_j)\delta(\mathbf{r}_j-\mathbf{r})\rangle. \tag{55}$$

Here, $P_2(x)$ is the second Legendre polynomial. We found that, with increasing polarity, the surface dipoles increasingly tend to orient orthogonal to the surface normal,[40] a behavior well documented for two-dimensional dipolar fluids[41] and cavities in force field water.[42] This orientational pattern results in overscreening of the external field, leading to the electric field from the first solvation shell directed opposite to the external field (Fig. 9). This overscreening is compensated by a positive field from the second solvation shell. The compensation is far from complete for small cavities, indicating that formation of a cavity field is a nonlocal event involving several solvation shells (Fig. 9). For larger cavities (not shown here), the fields of the two first solvation shells makes almost the entire cavity field such that the solvent response is more local. Still, overscreening present for large cavities implies that the continuum picture of an abruptly terminated polarization is inadequate at the length scale of two solvation shells. Even though one can argue that this scale is way below the scales considered by the macroscopic electrostatics, the simulations show that it is on this length scale where the polarization response is formed, while the rest of the liquid contributes relatively little to the net result. Therefore, a correct account of dipolar correlations on that microscopic length scale is critical for capturing the result, and it is in this incorrect account of surface correlations where the standard electrostatics fails.

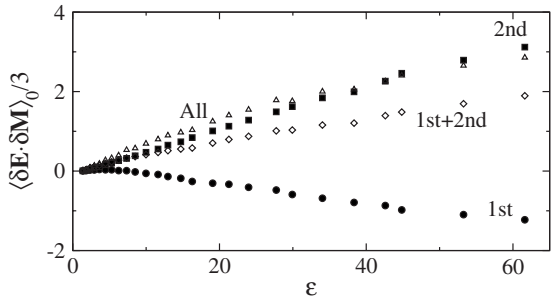

FIG. 9. The correlator $\langle\delta\mathbf{E}\cdot\delta\mathbf{M}\rangle_0/3$ from Eq. (48) calculated from MC simulations for the dipoles in the first solvation shell surrounding the cavity (circles), from the second solvation shell (squares), and from the entire simulation box (open triangles). The sum of contributions from the first and second solvation shells is indicated by open diamonds. The cavity radius is $R_1/\sigma=1.0$.

C. Reaction field

The simulation results for the reaction field inside cavities of different sizes are shown in Fig. 10 and listed in Table II in the supplementary material.[37] The simulated points fall significantly below the continuum result when R_0 is used for the cavity radius in Eq. (40). In addition, the microscopic reaction field does not saturate at $\epsilon\gg 1$ but instead keeps increasing approximately linearly with ϵ.[43] Nevertheless, the reaction field from simulations seems to get closer to the continuum Onsager result with increasing cavity size, and there are no dramatic qualitative discrepancies between the continuum and microscopic results, in contrast to the situation with the cavity field.

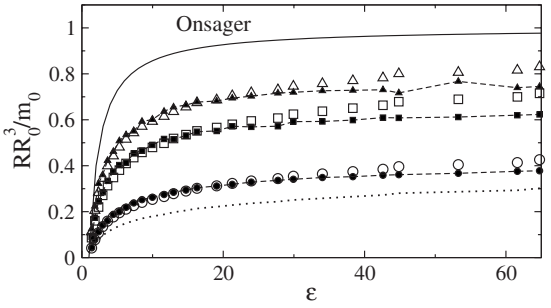

FIG. 10. Reaction field calculated from the continuum electrostatics [Eq. (40)] (solid line marked "Onsager," R_0 is used for the cavity radius) and from Eq. (39) (filled points) with the effective radius R_{eff} [Eq. (41)] used in place of R_1: $R_0=0.5$ (circles), 1.0 (squares), and 1.5 (triangles). The open points correspond to the MC simulation data for the same R_0 values as the closed points. The dotted line applies Eq. (39) at $R_0/\sigma=0.5$ with R_1 used for the cavity radius. The dashed lines connect the points and the structure factors from MC simulations were used for k integration in Eq. (39).

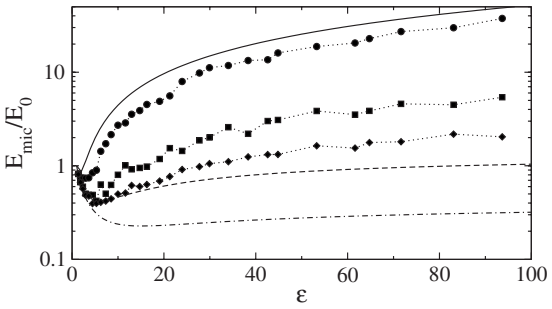

FIG. 11. Microscopic field at the position of the dipole m_0 at the center of a spherical cavity of radius R_0. The results at different ϵ were obtained for $R_0/\sigma=0.5$ (circles), 1.0 (squares), and 1.5 (diamonds) using Eq. (49). The solid line refers to the continuum prediction for the homogeneous liquid [Eq. (46)], while dashed and dashed-dotted lines refer to $R_0/\sigma=1.0$ and $R_0/\sigma=1.5$, respectively, obtained from Eq. (47).

The direct calculation of R by using Eq. (39) yields the reaction field qualitatively reproducing the results of the simulations but quantitatively too low. The reason for the deviation is well understood:[44] cutting out the polarization field from the solute volume in Eq. (11) does not incorporate the fact that other liquid fields, e.g., density, must also be zero inside the cavity. In particular, the coupling of the local density field around the cavity with the polarization field accounts for a stronger reaction field. This deficiency can be remedied in the mean-field fashion by replacing the radius of the closest approach R_1 in Eq. (39) with the effective radius R_{eff} from Eq. (41). This approach in fact gives results very close to the simulations (closed points in Fig. 10). Since the structure factors in such calculations are well approximated by the parametrized MSA solution,[31] the problem of calculating the reaction field in dipolar fluids from Eq. (39) reduces to a simple quadrature. A slight downward deviation of the analytical results from the simulations at high ϵ may be due to an effective decrease in the density of the liquid in contact with the cavity at high polarities in comparison with the result for the binary hard-sphere mixture.[43]

D. Microscopic field

Simulations of the microscopic field at the position of a probe dipole were done here at $m_0=m$ and varying dipole m^* and the cavity radius R_0. The results are listed in Table II in the supplementary material[37] and illustrated in Fig. 11 where E_{mic}/E_0 calculated from Eq. (49) (points) are plotted against ϵ. The simulation results are compared to the continuum predictions for the homogeneous liquid [Eq. (46)] and to Eq. (47) for the heterogeneous configuration with the cavity radius exceeding that of the solvent. The results for the homogeneous continuum [Eq. (46)] compare fairly well with the simulations. However, the continuum field is predicted to fall off rather sharply with increasing the cavity size, which is not supported by the simulations. The overall decay of the simulated microscopic field is much slower due to the cavity field much exceeding Maxwell's result at large ϵ (Fig. 7) and, in addition, a fairly weak decay of $g_K^{(0)}$ with increasing cavity size (Table II in the supplementary material[37]).

V. DISCUSSION

Condensed materials made of dipolar particles, independently of composition and phase, are often described by material Maxwell's equations.[9] These are a very successful mathematical construct which includes several components. First, the Maxwell macroscopic field in the absence of free charges satisfies the equation

$$\text{div } \mathbf{E} = -4\pi \text{ div } \mathbf{P}. \tag{56}$$

This relation comes as a mathematical property of the dipolar tensor used to build the Maxwell field from the external field $\mathbf{E}_0$ and the field of the bulk polarization:

$$\mathbf{E}(\mathbf{r}) = \mathbf{E}_0 - (4\pi/3)\mathbf{P}(\mathbf{r}) + \int_{|\mathbf{r}-\mathbf{r}'|<\delta} \mathbf{T}(\mathbf{r}-\mathbf{r}') \cdot \mathbf{P}(\mathbf{r}')d\mathbf{r}'. \tag{57}$$

Here, the second term eliminates the singularity of $\mathbf{T}(\mathbf{r})$ at $\mathbf{r}\to 0$ when Eq. (57) is used in the bulk.[36,45] Second, one needs the electrostatic constitutive relation,[45] that is, the proportionality between $\mathbf{E}(\mathbf{r})$ and $\mathbf{P}(\mathbf{r})$ [left-hand side of Eq. (2)], to arrive from Eq. (56) to the Poisson equation $\Delta\phi=0$ in the absence of free charges.

The constitutive relation assumes locality of the liquid response which does not hold at microscopic distances requiring a convolution with a nonlocal response function which can be expressed in terms of a k-dependent dielectric constant.[5,46–50] This convolution relation then replaces a simple proportionality which, however, is restored in inverted space. The convenience of working in inverted space requires, however, considering the longitudinal and transverse polarization responses separately, with quite different qualitative behavior of the corresponding response functions (Fig. 2). The symmetry breaking between the properties of the longitudinal and transverse responses is a basic consequence of the Coulomb law and its multipole expansion[10] [Eq. (57)] and has nothing to do with specific molecular interactions within dipolar systems.[51] This qualitative difference between the two types of response is the cause of many peculiarities of fields inside dielectrics which we have observed here since different fields carry different weights of the longitudinal and transverse components (see below).

Solving the Poisson equation for problems involving impurities (solvation) and interfaces requires imposing dielectric boundary conditions, which come as a second, independent of Eqs. (56) and (57), part of the theory. In Maxwell's dielectric, those are obtained by assuming that dipolar polarization abruptly terminates at the interface, thus creating a surface charge σ_i equal to the polarization component normal to the interface, $\sigma_i=P_n$.[4] This assumption might be of unequal relevance for different media. While it is probably more adequate for solid and amorphous materials with restricted freedom of dipolar rotations, it might be less applicable to fluid dielectrics where dipolar orientations are rearranged in response to the creation of the interface.[52] If the orientational dipolar structure of the liquid interface is significantly different from the abrupt discontinuity of Max-

well's dielectric, the boundary conditions of the Poisson equation might change, generating a new continuum solution at a large length scale.

In order to examine the applicability of Maxwell's boundary conditions to fluid dielectrics we have attempted here a bottom-up approach to the problem by starting with well-defined microscopic response functions of pure dipolar liquids [Eqs. (18)–(21)]. We then *derived* the continuum limit from microscopic equations instead of *assuming* that polar liquids should become Maxwell's dielectric at a large length scale. This latter assumption is a starting point of many previous approaches to liquid dielectrics.[28,53] By using this alternative approach we got a glimpse at the central question of this study: whether and how fast fluid dielectrics approach Maxwell's dielectric with increasing the length scale. It turned out that there is no uniform answer to this question as it depends on the property at hand.

From three dielectric fields considered here and in principle observable in the laboratory (E_d, E_c, R) the reaction field R seems to be best understood in terms of the standard electrostatics. There is a good physical reason for that. The dielectric response is fully determined by the properties of the solute and two response functions of the dipolar liquid, longitudinal and transverse (Fig. 2). From these two, the longitudinal function is flat at low k values and the transverse function is increasingly sharp with increasing dielectric constant. The longitudinal response is therefore described reasonably well by the standard electrostatics replacing the response function by its $k=0$ value. The applicability of the same approximation to the transverse response is questionable and is increasingly so with increasing liquid polarity.

The reaction field arises as a sum of longitudinal and transverse contributions to the solvation chemical potential [Eq. (37)]. The continuum limit predicts the dominance of the longitudinal over transverse response, with the weights 2:1 independent of ϵ.[26] This splitting would still suggest a possibility of a nonstandard solution when the transverse part of the response deviates from the continuum prediction at large ϵ. What happens instead is that the transverse component of the response is essentially eliminated when the full k integration of the structure factors is used in Eq. (37) instead of the continuum limit.[26] The overall polar response to a dipolar solute is therefore mostly longitudinal, and that explains the qualitatively adequate performance of the Onsager formula. The response is completely longitudinal by symmetry in the case of ion solvation, and that is why the celebrated Born[54] formula for solvation of a spherical ion is mostly a reliable approximation. The result is much less sensitive to the choice of the cavity radius compared to the dipole case, which is why the Born equation has received such enormous popularity in solution and computational chemistry.

The situation becomes radically different when one turns to the calculation of the cavity/directing field. As we have shown above, Eq. (31) becomes Maxwell's cavity field [Eq. (32)] if the continuum limit $k=0$ is taken in the response functions $\chi''^{L,T}(k)$. One needs to note that $\chi''^{T}(0)=3\epsilon/(2\epsilon+1)$ and $\chi''^{L}(0)=3/(2\epsilon+1)$. Therefore, this standard continuum limit suggests that deviations of the field inside a finite-size cavity from the Lorentz field applicable to an infinitely small cavity are determined by the transverse response. This latter is not adequately described by its continuum limit and that is the physical reason behind the problems we encountered here with the Maxwell cavity field. The simple algebraic transformation in Eq. (33) eliminates this dominance of the transverse response and allows a more reliable transition to continuum. The resulting cavity field [Eq. (34)] then turns out to be fairly close to the Lorentz field (see the solid and dashed lines in Fig. 12).

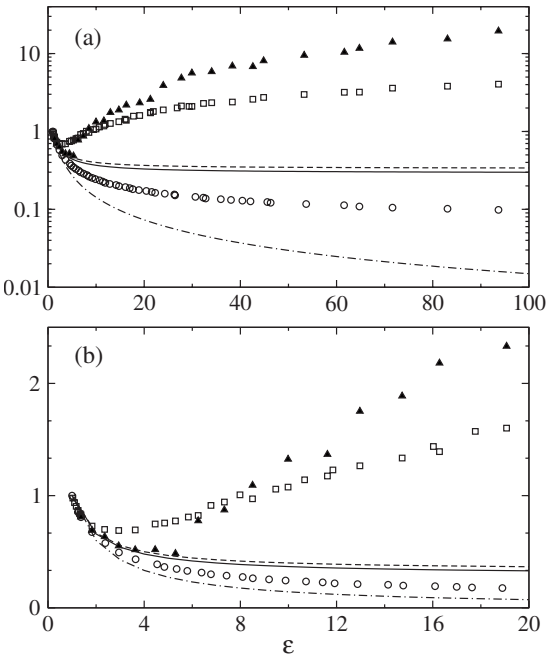

FIG. 12. The local E_{loc}/E_0 field [Eq. (3)] (circles), the cavity field E_c/E_0 (squares), and the directing field E_d/E_0 (closed triangles) vs ϵ for $R_0/\sigma=0.5$. The solid line indicates the new continuum cavity field [Eq. (34)], the dashed line is the Lorentz local field [Eq. (5)], and the dashed-dotted line is the Maxwell cavity field [Eq. (9)]. The lower panel is an expanded section at small ϵ.

Even though these arguments are easy to understand, the analytical development has produced an unexpected result of a real-axis singularity in the response functions,[26,40] showing that the solution might switch to Maxwell's result at high ϵ. This singularity signals the appearance of a macroscopic longitudinal polarization wave, making the solution sensitive to the conditions at the boundary of a macroscopic sample, as is the case with the standard Maxwell equations. Whether this polarization instability corresponds to polarized domain formation, seen in some laboratory[16,17] and computer[55] experiments, remains to be established. We have observed, however, that one needs to replace the continuous inverted-space integral with a lattice sum in order to avoid the real-axis singularity and maintain the "new continuum" solution. This procedure in fact constitutes a certain order in taking the thermodynamic, $N\to\infty$, and continuum, $k\to 0$, limits. The new continuum appears when the continuum limit is followed by the thermodynamic limit: $\lim_{N\to\infty}\lim_{k\to 0}\cdots$, while Maxwell's dielectric appears at large ϵ from the switched order of two limits: $\lim_{k\to 0}\lim_{N\to\infty}\cdots$. There is nothing in the theory that stipulates how these limits should be taken and, therefore, the right approach to continuum should be decided by laboratory measurements.

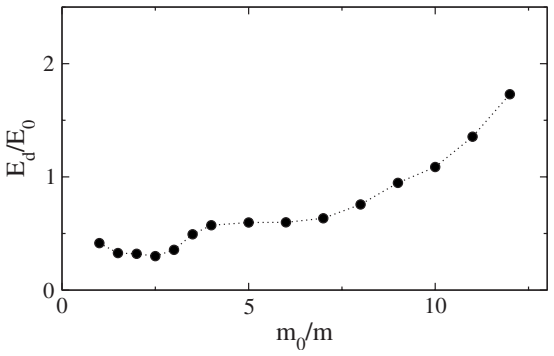

FIG. 13. Directing field vs the target dipole moment m_0/m. Points are simulations data at $(m^*)^2=1.0$, $R_0/\sigma=1.5$; the dotted line connects the points.

Before suggesting experimental tests in Sec. VI, we will comment on the comparison of the local, directing, and cavity fields from our simulations. Figure 12 compares the cavity, E_c, directing, E_d, and local, E_{loc}, fields. The cavity size in Fig. 12 is taken equal to that of the liquid particles in order to include the local field in the comparison. The local field [Eqs. (1) and (3)] is a mean-field construct, whereas the cavity and directing fields include all dipolar correlations without relying on the mean-field approximation. As is seen, all three are reasonably close at $\epsilon<3$ and then start to deviate from each other. The directing field first follows the Lorentz field [Fig. 12(b)] but then turns upward and starts to increase with ϵ faster than the cavity field. The local field is consistently below the other two at large ϵ, testifying to the long-known fact that mean-field models do not describe high-polarity dielectrics[22] [Eq. (10)].

VI. EXPERIMENTAL TESTS

Fields within fluid dielectrics have received significant attention from experiment over many decades of studying dielectric materials.[56] While the local field is a theoretical construct of mean-field models, the directing (E_d), reaction (R), and cavity (E_c) fields are real physical entities subject to experimental determination. The directing field is responsible for the torque rotating the dipole in linear or nonlinear dielectric experiments. The cavity field is probably harder to measure since one needs a small probe dipole within a large cavity to avoid altering the nature of orientational dipolar correlations at the cavity surface. However, our results suggest a fairly low sensitivity of the directing field to the magnitude of the target dipole m_0.

Figure 13 shows the results of simulations in which the directing field was calculated versus the target dipole m_0; the limit $m_0=0$ corresponds to the cavity field. In order to understand this plot, one needs to compare the effective coupling between the liquid dipoles, $(m^*)^2=1.0$, with the effective solute-solvent coupling, $(m_0/m)(m^*)^2(\sigma/R_1)^3=m_0/8m$. It is seen that the solute-solvent interaction energy becomes comparable to that between the solvent dipoles at the end of the scale of m_0/m values shown in Fig. 13. The directing field is about four times larger than the cavity field at that point. The plot also indicates that solute-solvent interactions below roughly 40% of the solvent-solvent interaction energies give directing fields fairly close to the cavity field. Therefore a sufficiently small dipole inside an impurity can be used to experimentally measure the cavity field.

The reaction field has probably been most studied experimentally since it can be directly related to the spectral shift of a dipolar optical probe dissolved in the liquid.[23,57] The general consensus in the literature is that the Onsager formula gives a qualitatively correct grasp of the problem, although the cavity size required to solvate a molecular probe is poorly defined and the use of the van der Waals volume for that purpose gives an overestimated value for the shift. In addition, the calculation of the temperature dependence of the spectral shift using the dielectric constant gives inadequate results since microscopic models are required to gain access to the solvation entropy.[44] Further, saturation of the polar response is not reached in a fast fashion predicted by the Onsager formula, which has some consequences for the solvation dynamics.[58] These subtleties aside, the basic electrostatic predictions, the increase in the reaction field with increasing solvent polarity and a linear scaling with m_0^2/R_{eff}^3, have been supported by the experimental evidence. This statement is also in line with our present and previous[26] findings which have not revealed fundamental difficulties with the application of the standard electrostatics to the reaction field.

The situation is quite different with the cavity and directing fields for the reasons discussed above. The standard result predicts that the cavity field essentially disappears because of screening in a high-polarity Maxwell dielectric [Eq. (32)]. On the contrary, it tends to a constant in the mesoscopic analytical model [Eq. (34)] and rises with ϵ as is seen in numerical simulations. Therefore, effectively no torque is expected to act on a probe dipole within a cavity carved in Maxwell's dielectric, while a substantial torque should remain if a polar liquid follows our present findings.

When asking how to test these results one might turn to the substantial experimental database on the cavity field produced by induced dipoles. This cavity field is probed by the intensity of an optical transition through the interaction of the transition dipole with the electric field of the radiation source.[59–61] However, the range of dielectric constants (squared refractive index) available in such experiments is very limited and, more importantly, that problem is physically distinct from our present agenda in which new solutions arise from orientational correlations of permanent molecular dipoles. Physically, induced dipoles are oriented along the field, while the orientational correlations between the permanent dipoles are only weakly perturbed by an external field. From this viewpoint, we are not aware of experimental effort to access the cavity field in strongly polar liquids. Here we provide some relations which can be used to interpret the results of laboratory measurements.

We first want to mention that the overall free energy of a uniformly polarized dielectric with N_c cavities in it does not depend on which solution for the cavity field is realized. From our microscopic response function [Eq. (13)] we find that the free energy ΔF of polarizing the dielectric is

$$\Delta F = -\tfrac{1}{2}\mathbf{E}_0 \cdot (\mathbf{M}_l + \mathbf{M}_c). \tag{58}$$

Here, $\mathbf{M}_l$ is the overall dipole moment of the uniformly polarized liquid with the polarization $\mathbf{P}$ before the cavities were introduced and $\mathbf{M}_c = -3\mathbf{P}V_c/(3\epsilon+1)$ is the dipole moment of N_c cavities occupying the overall volume V_c. This dipole moment is consistent with the solution of the Maxwell equations,[4] and thus our microscopic theory reproduces electrostatic results for the polarization free energy. From this equations, the standard arguments suggest that the dielectric constant of the liquid with cavities (ϵ_{mix}) is given as

$$\epsilon_{\mathrm{mix}} = \epsilon\left[1 + x_c\frac{3(\epsilon-1)}{2\epsilon+1}\right]^{-1}, \tag{59}$$

where x_c is the volume fraction of the cavities. Equation (59) appears to be the low-concentration limit of the Maxwell theory of dielectric mixtures.[56] Since the result is insensitive to the local cavity field, one has to introduce probe dipoles m_0 to probe the directing field E_d.

Once the probe dipoles m_0 are introduced inside the cavities, the time-dependent polarization of the mixture in response to a periodic external field $\mathbf{E}_0(t) = \mathbf{E}_0 \exp[i\omega t]$ can be given as

$$\mathbf{P}_{\mathrm{mix}}(t) = \mathbf{P}(t) + \mathbf{P}_c(t) + (N_c/V)\langle \mathbf{m}_0(t)\rangle, \tag{60}$$

where $\mathbf{P}(t)$ is the polarization of the homogeneous liquid and $\mathbf{P}_c(t)$ is the polarization due to cavities.

The probe dipoles are assumed to be sufficiently dilute so they do not interact. Their relaxation can be easily found from the linear response approximation,[62]

$$\langle \mathbf{m}_0(t)\rangle = (\beta m_0^2/3)\mathbf{E}_d(\omega)e^{i\omega t}[1 - i\omega\Phi(-\omega)], \tag{61}$$

where $\Phi(-\omega)$ is the Fourier–Laplace transform of the normalized correlation function,

$$\Phi(t) = m_0^{-2}\langle \mathbf{m}_0(t)\cdot\mathbf{m}_0(0)\rangle, \tag{62}$$

and $\mathbf{E}_d(\omega)$ is the directing field at the frequency ω. Combining Eqs. (59)–(61), one finds for the frequency-dependent response of the mixture

$$\epsilon_{\mathrm{mix}}^{-1}(\omega) = \epsilon(\omega)^{-1}\left(1 + x_c\frac{3(\epsilon(\omega)-1)}{2\epsilon(\omega)+1}\right) - 8(m_0^*)^2 x_c(E_d(\omega)/E_0)[1 + i\omega\tau_0]^{-1}, \tag{63}$$

where the Debye form $\Phi(\omega) = 1/(\tau_0^{-1} + i\omega)$ has been assumed for the rotational dynamics of the probe dipole and $(m_0^*)^2 = \beta m_0^2/(2R_0)^3$. From this equation, dielectric measurements of mixtures can potentially be used to get access to the magnitude of the directing field acting on a probe dipole.

VII. CONCLUSIONS

In conclusion, we have studied the cavity, directing, and reaction fields in liquid dielectrics by means of liquid-state theories and numerical simulations. Instead of demanding that the fields produced by liquid dielectrics in large-scale cavities must coincide with the fields produced by Maxwell's dielectric, we continuously increased the size of the spherical cavity to reach the continuum limit. Both simulations and analytical theory suggest that the commonly applied Onsager formula for the reaction field is approached from below by the microscopic solution with the increasing cavity size. On the contrary, the cavity and directing fields do not converge to the limit of Maxwell's dielectric. Instead, the cavity field obtained from simulations tends, with increasing cavity size, to the limit derived from our analytical theory. The origin of the disagreement between the continuum reached from microscopic models and that calculated from the standard electrostatics is traced back to the failure of the latter to account properly for the transverse correlations between the dipoles in molecular liquids. Among other things, this observation implies that experimental setups avoiding the transverse response (e.g., the familiar plane capacitor) will not detect qualitative inconsistencies with the Maxwell electrostatics.

ACKNOWLEDGMENTS

This research was supported by the NSF (Grant No. CHE-0616646).

[1] J. C. Maxwell, *A Treatise on Electricity and Magnetism* (Dover, New York, 1954), Vol. 2.
[2] P. Mazur, Adv. Chem. Phys. **1**, 309 (1958).
[3] V. L. Ginzburg, Phys. Usp. **44**, 1037 (2001).
[4] C. J. F. Böttcher, *Theory of Electric Polarization* (Elsevier, Amsterdam, 1973), Vol. 1.
[5] O. V. Dolgov, D. A. Kirzhnits, and E. G. Maksimov, Rev. Mod. Phys. **53**, 81 (1981).
[6] F. O. Raineri and H. L. Friedman, Adv. Chem. Phys. **107**, 81 (1999).
[7] L. Onsager, J. Am. Chem. Soc. **58**, 1486 (1936).
[8] G. Stell, G. N. Patey, and J. S. Høye, Adv. Chem. Phys. **48**, 183 (1981).
[9] L. D. Landau and E. M. Lifshitz, *Electrodynamics of Continuous Media* (Pergamon, Oxford, 1984).
[10] J. D. Jackson, *Classical Electrodynamics* (Wiley, New York, 1999).
[11] D. Wei and G. N. Patey, Phys. Rev. Lett. **68**, 2043 (1992).
[12] B. Huke and M. Lücke, Rep. Prog. Phys. **67**, 1731 (2004).
[13] J. Bartke and R. Hentschke, Mol. Phys. **104**, 3057 (2006).
[14] D. Wei, G. N. Patey, and A. Perera, Phys. Rev. E **47**, 506 (1993).
[15] J. M. Luttinger and L. Tisza, Phys. Rev. **70**, 954 (1946).
[16] D. P. Shelton and P. Kaatz, Phys. Rev. Lett. **84**, 1224 (2000).
[17] D. P. Shelton and Z. Quine, J. Chem. Phys. **127**, 204503 (2007).
[18] M. A. Pounds and P. A. Madden, J. Chem. Phys. **126**, 104506 (2007).
[19] J. D. Ramshaw, J. Chem. Phys. **57**, 2684 (1972).
[20] J. S. Høye and G. Stell, J. Chem. Phys. **61**, 562 (1974).
[21] J. S. Høye and G. Stell, Mol. Phys. **86**, 707 (1995).
[22] K. I. Morozov, J. Chem. Phys. **119**, 13024 (2003).
[23] N. Mataga and T. Kubota, *Molecular Interactions and Electronic Spectra* (Marcel Dekker, New York, 1970).
[24] H. Li and M. Kardar, Phys. Rev. A **46**, 6490 (1992).
[25] D. Chandler, Phys. Rev. E **48**, 2898 (1993).
[26] D. V. Matyushov, J. Chem. Phys. **120**, 1375 (2004).
[27] P. Madden and D. Kivelson, Adv. Chem. Phys. **56**, 467 (1984).
[28] H. Fröhlich, *Theory of Dielectrics* (Oxford University Press, Oxford, 1958).
[29] M. S. Wertheim, J. Chem. Phys. **55**, 4291 (1971).
[30] C.-K. Duan, M. F. Reid, and Z. Wang, Phys. Lett. A **343**, 474 (2005).
[31] D. V. Matyushov, J. Chem. Phys. **120**, 7532 (2004).
[32] B. Linder and D. Hoernschemeyer, J. Chem. Phys. **46**, 784 (1967).
[33] D. V. Matyushov and B. M. Ladanyi, J. Chem. Phys. **110**, 994 (1999).
[34] S. Gupta and D. V. Matyushov, J. Phys. Chem. A **108**, 2087 (2004).
[35] M. P. Allen and D. J. Tildesley, *Computer Simulation of Liquids* (Clarendon, Oxford, 1996).
[36] M. Neumann, Mol. Phys. **57**, 97 (1986).
[37] See EPAPS Document No. E-JCPSA6-129-017841 for the results of the dielectric field simulations and the description of the simulation protocol. For more information on EPAPS, see http://www.aip.org/pubservs/epaps.html.
[38] A. Tani, D. Henderson, and J. A. Barker, Mol. Phys. **48**, 863 (1983).
[39] J.-J. Weis, J. Chem. Phys. **123**, 044503 (2005).
[40] D. R. Martin and D. V. Matyushov, Europhys. Lett. **82**, 16003 (2008).

[41] J. J. Weis, Mol. Phys. **100**, 579 (2002).
[42] S. Rajamani, T. Ghosh, and S. Garde, J. Chem. Phys. **120**, 4457 (2004).
[43] A. Milischuk and D. V. Matyushov, J. Phys. Chem. A **106**, 2146 (2002).
[44] D. V. Matyushov, Chem. Phys. **174**, 199 (1993).
[45] J. D. Ramshaw, J. Chem. Phys. **55**, 1763 (1971).
[46] A. A. Kornyshev, in *The Chemical Physics of Solvation*, edited by R. R. Dogonadze, E. Kálman, A. A. Kornyshev, and J. Ulstrup (Elsevier, New York, 1985), Vol. 1, p. 77.
[47] M. S. Skaf and B. M. Ladanyi, J. Chem. Phys. **102**, 6542 (1995).
[48] P. A. Bopp, A. A. Kornyshev, and G. Sutmann, Phys. Rev. Lett. **76**, 1280 (1996).
[49] I. P. Omelyan, Mol. Phys. **93**, 123 (1998).
[50] B.-C. Perng and B. M. Ladanyi, J. Chem. Phys. **110**, 6389 (1999).
[51] D. Kivelson and H. Friedman, J. Phys. Chem. **93**, 7026 (1989).
[52] V. P. Sokhan and D. J. Tildesley, Mol. Phys. **92**, 625 (1997).
[53] G. Nienhuis and J. M. Deutch, J. Chem. Phys. **55**, 4213 (1971).
[54] M. Born, Z. Phys. **1**, 45 (1920).
[55] G. Karlström, J. Phys. Chem. B **111**, 10745 (2007).
[56] B. K. P. Scaife, *Principles of Dilectrics* (Clarendon, Oxford, 1998).
[57] L. Reynolds, J. A. Gardecki, S. J. V. Frankland, and M. Maroncelli, J. Phys. Chem. **100**, 10337 (1996).
[58] D. V. Matyushov, J. Chem. Phys. **122**, 044502 (2005).
[59] J. E. Lewis and M. Maroncelli, Chem. Phys. Lett. **282**, 197 (1998).
[60] J. U. Andersen and E. Bonderup, Eur. Phys. J. D **11**, 435 (2000).
[61] G. M. Kumar, D. N. Rao, and G. S. Agarwal, Phys. Rev. Lett. **91**, 203903 (2003).
[62] J. P. Hansen and I. R. McDonald, *Theory of Simple Liquids* (Academic, Amsterdam, 2003).